Microchimica Acta (2019) 186: 788
https://doi.org/10.1007/s00604-019-3974-8

ORIGINAL PAPER

Cysteamine-capped gold-copper nanoclusters for fluorometric determination and imaging of chromium(VI) and dopamine

Muthaiah Shellaiah[1] · Turibius Simon[2] · Natesan Thirumalaivasan[1] · Kien Wen Sun[1] · Fu-Hsiang Ko[2] · Shu-Pao Wu[1]

Received: 10 June 2019 / Accepted: 25 October 2019 / Published online: 15 November 2019
© Springer-Verlag GmbH Austria, part of Springer Nature 2019

Abstract

Highly emissive cysteamine-capped gold-copper bimetallic nanoclusters (**CA-AuCu NCs**) with a quantum yield of 18% were synthesized via one-pot anti-galvanic reduction. The **CA-AuCu NCs** were characterized by HR-TEM, XPS, FTIR, MALDI-TOF mass spectrometry, DLS, and zeta potential analyses. The NCs are shown to be viable fluorescent probes for Cr(VI) ions and dopamine (DA) via quenching of the blue fluorescence, typically measured at excitation/emission wavelengths of 350/436 nm. During DA recognition, a dark brown color appears, which is distinguishable from that of Cr(VI) detection. The aggregation induced quenching due to electron transfer was demonstrated by photoluminescence, HR-TEM, FTIR, DLS, and zeta potential interrogations. In buffer of pH 7, response is linear in the 0.2 ~ 100 μM for Cr(VI) and from 0.4 ~ 250 μM for DA. The respective detection limits are 80 and 135 nM. The method was applied to the determination of both Cr(VI) and DA in (spiked) tap, lake and sea water, and in human urine samples. The low toxicity of **CA-AuCu NCs** was validated by the MTT assay, and their responses to Cr(VI) ions and DA was also proven by Raw 264.7 cell imaging.

Keywords Au-cu alloy · Neurotransmitter · Cr(VI) detection · Colorimetric sensor · Particle aggregation · Static quenching · Nanomolar detection · Cell imaging · Spiked urine investigation · Real analysis

Introduction

Attributed to the toxicity and World Health Organization (WHO) restriction on permitted level of Cr(VI) ions than those of Cr(III) ions, the development of diverse probes for its selective and sensitive detection is still in need [1, 2]. In a similar trend, due to prominence role over several nervous functions, determination of Dopamine (DA; a catecholamine derivative) is also become vital [3]. The presence of toxic Cr(VI) ions and abnormal or insufficient levels of DA might led to severe disease, such as DNA damage, Alzheimer's disease, depression, schizophrenia, and Parkinson's disease [4–6]. Therefore, many analytical techniques have emerged for Cr(VI) and DA quantifications. For example, Cr(VI) ions quantifications can be done by gas chromatography, inductively coupled plasma mass spectrometry, atomic absorption spectrometry, and electrochemical studies [7, 8]. On the other hand, DA can be detected through voltametric analysis, chromatographic techniques, and immunoassays [9, 10]. Similar to those conventional methods, the design of fluorescent probes for Cr(VI) and DA detection are still an analytical challenge due to the orthodox sample preparation, high sensitivity and imaging applicability [11].

Luminescent nanomaterials, such as carbon dots (C-dots), quantum dots (QDs), and metallic nanoclusters (MNCs), display the inspiring detection of Cr(VI) ions and DA in biological and environmental samples [12–17]. For instance, Mutuyimana et al., described the yellow emissive C-dots for the detection of Cr(VI) ions in fish and shrimps [18]. Similarly, Cui et al., presented the fluorescent iridium nanoclusters (IrNCs) for the effective determination of Cr(VI) ions in real samples [19]. On the other hand, a fluorometric based assay of DA in serum and cell imaging studies was reported by aptamer-functionalized Molybdenum

Electronic supplementary material The online version of this article (https://doi.org/10.1007/s00604-019-3974-8) contains supplementary material, which is available to authorized users.

✉ Kien Wen Sun
kwsun@mail.nctu.edu.tw

[1] Department of Applied Chemistry, National Chiao Tung University, Hsinchu 300, Taiwan

[2] Department of Materials Science and Engineering, National Chiao Tung University, Hsinchu 300, Taiwan

disulfide (MoS_2) QDs and nanosheets [20]. However, there is no report so far on bimetallic-nanoclusters (bi-MNCs) based simultaneous detections of Cr(VI) ions and DA, which provides us an initiative to proceed in that direction.

Bi-M NCs usually can be developed by following methods: (1) galvanic exchange; (2) anti-galvanic reduction; (3) thiol-etching of bi-metallic nanoparticles; (4) re-organization of bi-metallic species; (5) potential deposition [21]. Among them, anti-galvanic reduction tactic is quite impressive and provides highly emissive bi-M NCs [22]. For example, Sun and co-workers suggested the one-pot synthesize of 11-mercaptoundecanoicacid (11-MUA) capped Ag/Au bimetallic nanoclusters with 6.81% Φ value via anti-galvanic reduction and employed as pH sensors [23]. Similar to 11-MUA, cysteamine (CA) can also act as an effective stabilizer of M NCs or bi-M NCs through M-S bond and afford free amine ($-NH_2$) for particular analyte detection [24]. Therefore, by adapting the anti-galvanic reduction methodology and utilizing cysteamine as ligand, it is possible to develop cysteamine capped gold-copper nanoclusters (**CA-AuCu NCs**) as a chemosensory probe.

In this report, **CA-AuCu NCs** are developed with strong blue emission (Φ = 18%) via one pot anti-galvanic reduction. Upon exposure to metal ions and aminoacids, the **CA-AuCu NCs** reveal great selectivity to Cr(VI) ions and DA through aggregation mediated static quenching mechanism. In this study, the sensory responses of the **CA-AuCu NCs** are well authenticated in real, spiked urine and cellular imaging investigations.

Experimental

The general information on stock solutions, Instruments used, sample preparation procedures for TEM, FTIR, XPS studies, MTT assay and cell imaging protocols of **CA-AuCu NCs**, **CA-AuCu NCs** + Cr(VI) and **CA-AuCu NCs** + DA with corresponding data are delivered in Electronic Supporting Material (ESM).

Synthesize of CA- AuCu NCs [23]

4 mL of 10 mM Tetrachloroauric acid ($HAuCl_4$) and 40 μL of 10 mM copper nitrate ($CuNO_3$) were added into 31.96 mL of DI water solution (final volume 40 mL) and stirred at 55^0 C for 30 min to obtain the homogeneous mixture. 4 mL of 1 M cysteamine (CA) was dropped into above homogeneous solution within 5 min and then cooled down to room temperature. Subsequently, 12 mL of 1 M sodium hydroxide (NaOH) was added and stirred at room temperature for 3 h. After that, the mixture was stirred at 70^0 C for 0 to 72 h. Finally, to rid out the excess $HAuCl_4$, CA and NAOH, the luminescent **CA-AuCu NCs** solution was subjected to centrifugation and several water washing at 3500 rpm for 1 h. The **CA-AuCu NCs** were re-dispersed in DI water (25 mg/100 mL) and stored in refrigerator at 4 °C for further use.

Protocol for determination of Cr(VI) and DA

Deionized water (DI), laboratory tap water, NCTU Lake and Pacific Ocean Sea (located in Hsinchu, Taiwan) water samples were collected and filtered over a 0.2 μm membrane. From standard solutions (10, 100 and 1000 μM) of Cr(VI) ions, different volumes were spiked in to 200 μL of DI/lake/tap/sea water samples and subjected to PL based assay. Those samples were added to the solution containing 25 μg of **CA-AuCu NCs** dispersed in DI water and 400 μL of HEPES (pH -7) buffer. The diverse concentrations of Cr(VI) ions were made-up in respective DI/real water samples and spiked to the above **CA-AuCu NCs** in HEPES (pH -7) buffer. Next, the PL spectra were recorded after 15 min at room temperature. The results of above conventional sensing method were compared with ICP-MS analysis. For DA assay, similar procedure was followed by accumulating various concentrations of DA standard solutions (1 and 10 mM) in respective DI/real water samples to **CA-AuCu NCs** in HEPES (pH -7), incubated for 2 h at room temperature and the PL spectra were recorded. For both Cr(VI) and DA assay, the excitation wavelength was set at 350 nm; excitation and emission slits were fixed as 5 nm and the PL recorded between 400 to 600 nm ranges.

Spiked human urine analysis

For practical applications, the detection of Cr(VI)/DA were done in spiked human urine sample inquiry by standard addition method agreed with related reports [25, 26]. Before the analysis, urine samples were diluted 150 times with distilled water to decrease the matrix effect. No other pre-treatment was executed. Thereafter, above declared procedure was followed for urine based detection of Cr(VI) ions or DA, which was further investigated by PL spectra. The excitation wavelength was at 350 nm with excitation and emission slits fixed as 5 nm and the PL was recorded between 400 to 600 nm ranges.

Results and discussion

Choice of materials

Cysteamine (CA) was chosen as a stabilizer consist of free thiol (-SH) that can functionalize over metal surface through M-S bond and remnants free amine ($-NH_2$) group to

coordinate with specific analyte. Based on galvanic series, noble Au and Cu atoms were selected at 100:1 (Au/Cu) molar ratio to produce highly emissive **CA-AuCu NCs**. To induce effective anti-galvanic reduction, 1 M NaOH was used as a basic medium, which improved nanostructure affordability and galvanic exchange. Furthermore, the comparable low toxicity, stability and electronic structure of **CA-AuCu NCs** than those of well-known C-dots, semiconductor QDs and noble NPs make them more favourable for practical use. Note that, contrary to colorimetric responses of noble NPs, **CA-AuCu NCs** can be applied in fluorometric assays.

Synthesis and characterization of CA-AuCu NCs

As shown in Fig. 1, the **CA-AuCu NCs** are synthesized via one-pot anti-galvanic reduction [23]. But, **CA-AuCu NCs** with high fluorescent quantum yield (Φ) are attained through optimization of $HAuCl_4$, $CuNO_3$, Cysteamine (CA), and NaOH concentrations, as well as reaction time. Overall, the best emissive results of **CA-AuCu NCs** were accomplished at (1) 436 nm under excitation wavelength at 350 nm (see Fig. S1a and Table S1, ESM); (2) 1:0.1:100:300 equivalents of $HAuCl_4$: $CuNO_3$: Cysteamine (CA): NaOH, respectively (see Table S2, ESM); (3) after 48 h reaction time (see Fig. S1b and Table S2, ESM). Compared to Riboflavin monophosphate (Φ = 26.8% in water), the **CA-AuCu NCs** possess the Φ value of 18%. Increase of excitation wavelengths from 310 to 380 nm induced red shift of PL peaks because the electrons stimulated to the lower energy level relaxed and then produced emission at longer wavelengths.

The FTIR spectra of **CA-AuCu NCs** (Fig. S2, ESM) confirm the cysteamine functionalization via more diverse peaks than that of cysteamine. Wherein, the –CH and $–NH_2$ bands are broadened between 2950 ~ 3600 cm^{-1} and the –NH asymmetric stretching occurs at 1670 cm^{-1} instead of at 1612 cm^{-1} (as in the case of the CA). Above stretching bands also confirm the possible free $–NH_2$ groups. On the other hand, the free thiol (-SH) band of Cysteamine at 2569 cm^{-1} is almost vanished for the **CA-AuCu NCs**, hence confirmed the (Au-Cu)-S bond formation [27]. The HR-TEM image (Figs. S3a, ESM) confirms that the **CA-AuCu NCs** have a size between 1~5 nm [28]. However, among selected 100 particles, more than 50% have an average size of 3 nm as displayed in Fig. S3b (ESM). Besides, from Figs. S3c and d (ESM), the diffraction value is estimated as 0.218 which lies between the values of Au and Cu and is in good agreement with the 111 pattern of the Au-Cu alloy [29]. Moreover, DLS studies reveal an average size of 4.6 ± 3.3 nm for the **CA-AuCu NCs** (Fig. S4, ESM), which is fairly similar to the HR-TEM results. Next, zeta potential (ζ) of **CA-AuCu NCs** is established as −12.76 mV, (Fig. S5, ESM) and hence can be stabilized via –Ve repulsive force between particles.

As seen in Fig. S6 (ESM), the Maldi-Tof of **CA-AuCu NCs** give m/z values of 1883.47 and 2136.56, which can be related to $CA_{10}Au_5Cu_2$ NCs and $CA_{10}Au_5Cu_5$ NCs, respectively. However, it is well recognized that the majority of NCs have the molecular structure of $CA_{10}Au_5Cu_2$ NCs and it also confirms the cysteamine capping over Au-Cu alloy surface [30]. Results from the XPS of **CA-AuCu NCs** demonstrate the presence of Au4f, Cu2p, S2p, C1s, and N1 s peaks (Fig. S7a, ESM). The Au4f peaks occur at 84.8 eV ($4f_{7/2}$) and 88.4 eV ($4f_{5/2}$) as displayed in Fig. S7b (ESM). Likewise, Cu2p peak at 935.6 eV ($2p_{3/2}$) can be clearly seen in Fig. S7c (ESM). However, due to deficient amount of Cu atoms, the peak of $2p_{1/2}$ was not observed. It is noteworthy that the absence of the satellite peak at 941.9 eV (associated with the Cu^+) also confirms its clusterification [31]. The appearance of the S2p, C1s, and N1 s peaks at 164.4, 284.7, and 401.8 eV (Figs. S7d-f, ESM), correspondingly, proves the existence of S, C and N atoms over Au-Cu alloy. Due to the possible formation of (Au-Cu)-S bond, the S2p peak is strongly affected, hence confirms the cysteamine functionalization.

Analytical responses of CA-AuCu NCs

Initially, 300 μM of numerous metal ions [Na(I), Ni(II), Fe(III), Cd(II), Ca(II), Ga(III), Cr(III), Y(III), Cu(III), Fe(II), Mg(II) Ba(II), Au(III), Ag(I), Co(II), Zn(II), Pb(II), Sn(II), Al(III), Cr(VI) and Hg(II)] or 3 mM of other bio-analytes (Glucose, Cysteine, Homo-Cysteine, Lysine, Melamine, Glutamic Acid, Histidine, Tyrosine, Sucrose, Ornithine, Arginine, Ascorbic Acid, Glycine, Urea; Dopamine and

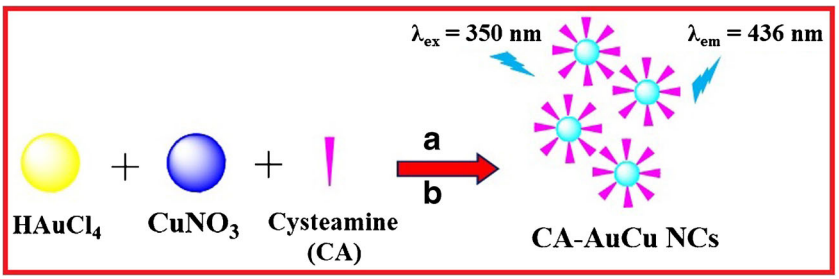

Fig. 1 Synthesis of **CA-AuCu NCs**; **a** 55^0 C, Cysteamine (CA), RT, 3 Hrs; **b** Stir at 70^0 C, 48 Hrs

Glutathione) were added to the **CA-AuCu NCs** solution in DI water and the respective fluorescence changes were recorded subsequently. The above investigations reveal excellent fluorescence quenching to Cr(VI) ions and DA than that of other interferences as shown in Fig. 2a and b. Under UV-lamp irradiation at 365 nm, the visual changes are clearly demonstrated by the photo images [Figs. 2a, b (insets), S8 and S9 (ESM)]. During the discovery of DA, a dark brown color is observed visually as shown in Fig. S9a (ESM). By studying different combinations of pH, concentrations of probe/analyte, and incubation time [Figs. S10-S12 (ESM)], the best sensory result was identified at (1) pH -7 HEPES buffer; (2) 25 μg/mL of **CA-AuCu NCs** concentration; (3) 300 μM and 1 mM of Cr(VI) and DA, individually (4) 15 min and 2 h incubation time for Cr(VI) and DA detection, respectively.

Next, the exceptional sensitivity of **CA-AuCu NCs** to Cr(VI) and DA is demonstrated by single and dual analyte studies in HEPES buffer (pH 7). In contrast to the remaining interferences, the **CA-AuCu NCs** show remarkable selectivity towards Cr(VI) and DA with 12 and 25 folds of PL quenching, respectively, as seen in Figs. S13a and b (ESM). At 1:5 ratio [Cr(VI) to other interferences], except the mild effect Al^{3+} and Cr^{3+} ions (7 folds quenching), none of other metal ions reveal any interfering effect on Cr(VI) selectivity as displayed in Fig. S14 (ESM). On the other hand, in the presence of all other metal ions, the PL quenching is enhanced between 20 120 folds.

In a similar fashion, at 1:3 ratio (DA to other interferences), except Ascorbic acid (AA; 3.9 folds quenching) and Tyrosine (Tyr; 3.7 folds quenching), none of other interferences affect the selectivity of DA as shown in Fig. S15 (ESM). However, at 1:1 mixing ratio of AA or Tyr, the selectivity of **CA-AuCu NCs** is not strongly affected and still displays 16 folds in PL quenching. This may be attributed to the structural similarity or redox potential similarity of both AA and Tyr to DA, and hence interfere the selective quenching. In particular, with excess amount of AA and Tyr, the -OH of Tyr and two similar –OH groups of AA may exceptionally interfere the electron transfer between catechol of DA to **CA-AuCu NCs** involved in the sensing mechanism. Therefore, to attain the reliable results with **CA-AuCu NCs**, complex samples containing excess of AA and Tyr should be avoided. From Figs. S16a and b (ESM), the Stern-Volmer Quenching Constant (K_{SV}) values [32] of **CA-AuCu NCs** + Cr(VI) and **CA-AuCu NCs** + DA are calculated to be 8.26×10^4 and 2.426×10^4 M^{-1}, correspondingly. Moreover, linearity in fluorescent responses of **CA-AuCu NCs** by Cr(VI) and DA also demonstrates the feasible static quenching. As noted in Tables S3 and S4 (ESM), the K_{SV} values of residual metal ions and bio-interferences oscillate between $10^2 \sim 10^3$ M^{-1}, hence proves the selective discrimination of Cr(VI) and DA.

Upon the accumulation of Cr(VI) ions (0 ~ 300 μM) or DA (0 ~ 1 mM) to **CA-AuCu NCs** in HEPES buffer (pH 7), the fluorescent peak at 436 nm is linearly quenched as depicted in Figs. 3a and b. In accordance with the above PL changes, the Φ values of **CA-AuCu NCs** + Cr(VI) and **CA-AuCu NCs** + DA are also reduced to 0.43 and 1.5%, respectively. From these titrations, linear regressions of Cr(VI and DA are adopted as 0.2 100 and 0.4 250 μM, correspondingly, as seen in Figs. 3c and d. By following the 3σ (signal to noise) and the linear regression equations of $y = 0.00788x + 2.53566 \times 10^{-4}$ ($R^2 = 0.98873$, $n = 4$) and $y = 0.01806x + 5.81193 \times 10^{-4}$ ($R^2 = 0.9867$, $n = 4$), the LODs of Cr(VI) ions and DA are calculated as 80 and 135 nM, respectively, which is below the prescribed limits by WHO.

Mechanism involved in Cr(VI) and DA detections

The presence of Cr(VI) ions and DA induced aggregation of **CA-AuCu NCs** are visualized in Figs. S17a and b (ESM). Similarly, for **CA-AuCu NCs** + Cr(VI) and **CA-AuCu NCs** + DA systems [Figs. S18a and b (ESM)], particle sizes of 129.9 ± 34.8 and 179.7 ± 51.1 nm determined by DLS are 28 and 39 folds larger than that of origin, respectively. Therefore, aggregation induced fluorescent quenching phenomena may possibly involve in Cr(VI) and DA detection [33], which can be further enhanced by manipulating the binding forces via FTIR interrogations. During the Cr(VI) recognition, free $–NH_2$ band of **CA-AuCu NCs** at 3000 3500 cm^{-1} (shown in Fig. S19a, ESM) is broadened along with the

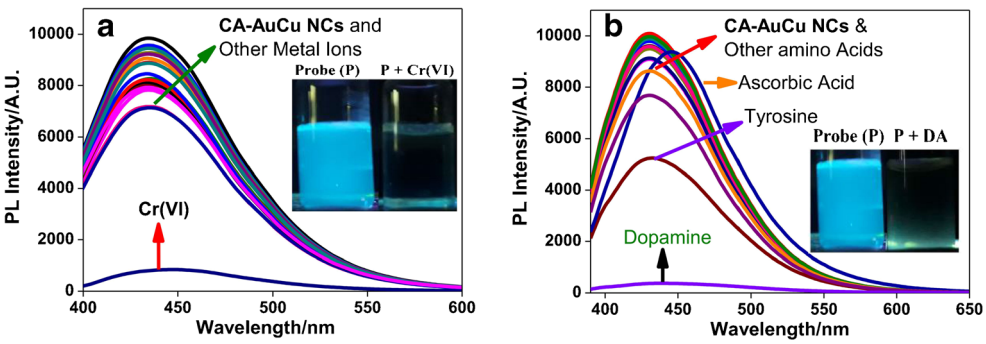

Fig. 2 **a** Fluorescence responses of **CA-AuCu NCs** towards metal ions ($\lambda_{ex/em} = 350/436$ nm); Inset: PL change by Cr(VI) ions (under UV lamp, $\lambda_{ex} = 365$ nm); **b** Fluorescence responses of **CA-AuCu NCs** towards dopamine (DA) and other interferences ($\lambda_{ex/em} = 350/436$ nm); Inset: PL change by DA (under UV lamp, $\lambda_{ex} = 365$ nm)

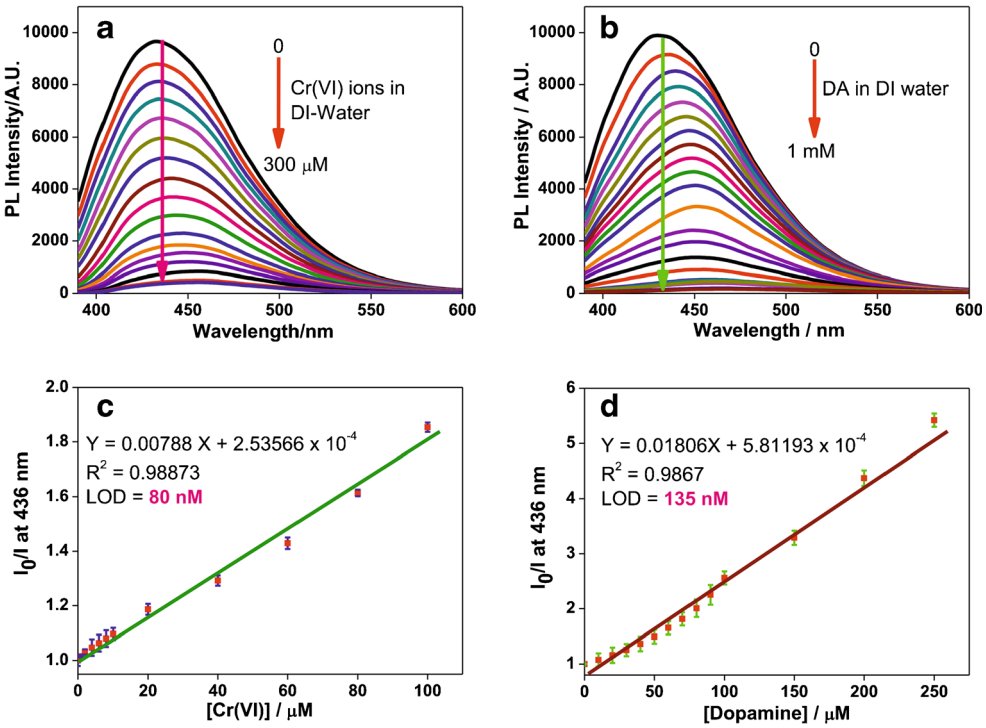

Fig. 3 **a** PL changes of **CA-AuCu NCs** in HEPES buffer (pH -7) with Cr(VI) ions (0 to 300 μM; $\lambda_{ex/em}$ = 350/436 nm); **b** PL changes of **CA-AuCu NCs** in HEPES buffer (pH -7) with dopamine (DA; 0 to 1 mM; $\lambda_{ex/em}$ = 350/436 nm); **c**, **d** detection limits (LODs) of Cr(VI) ions and DA calculated via standard deviation and fittings (n = 4; $\lambda_{ex/em}$ = 350/436 nm)

affected symmetric or asymmetric stretching bands. Hence, it indicates that coordination possibly takes place between free –NH_2 groups and Cr(VI) ions. In contrast, FTIR spectrum of **CA-AuCu NCs** + DA is completely broadened with mild shifting of –NH symmetric /asymmetric bands (Fig. S19b, ESM), which suggests feasible diverse mechanism. As reported earlier, the **CA-AuCu NCs** may attract the two acidic catechol protons of DA to form the stable phenoxide-enolate equilibrium [34] and lead to –Ve charge over aromatic ring and charge transfer between **CA-AuCu NCs** and DA to induce fluorescent quenching or ACQ. The aforementioned mechanisms are authenticated by zeta potential (ζ) data. For **CA-AuCu NCs** + Cr(VI), ζ value is shifted to +14.12 mV (Fig. S20, ESM) compared to that of −12.76 mV for **CA-AuCu NCs**, which supports the feasible coordination of free –NH_2 with Cr(VI) ions. Likewise, due to the diverse mechanism on DA determination, +Ve ζ value (+19.00 mV) is observed as shown in Fig. S21 (ESM). Finally, based on the TEM, DLS, FTIR, and zeta potential studies, these mechanisms are schematically illustrated in Figs. S22, and S23 (ESM).

Determination of Cr(VI) and DA

The distinct quantifications of Cr(VI) and DA can be done as follows. (1) At 200 μM concentration, Cr(VI) ions induce rapid fluorescent quenching than that of DA, which only prompt colorimetric response (colorless to dark brown); (2) Contrast to Cr(VI), higher concentration of DA (3 mM) is required to achieve immediate fluorescence quenching; (3) Consecutive addition of EDTA to **CA-AuCu NCs** + Cr(VI), the fluorescence recovered and extended up to four cycles (Figs. S24a-c, ESM). Above reversibility is effective at mixed states [Cr(VI) ions(200 μM) and DA (200 μM) with **CA-AuCu NCs**] as demonstrated in Figs. S25a and b (ESM).

Real and human fluid analysis

As presented in Table 1, the results of **CA-AuCu NCs** towards Cr(VI) in real and urine samples are in good agreement with ICP-MS data with less than 2.17% relative error. The recovery values of Cr(VI) ions in tap, lake, sea, and urine water fall between 110.42~116.01%, 109.03~116.41%, 106.22~114.03%, and 110.29~118.02%, correspondingly. Similarly, the PL based recovery of DA shows a relative error of less than 3.42% as shown in Table 2. The recovery values of DA in Tap, Lake, Sea, and Urine water lie between 99.78~100.33%, 98.45~101.45%, 98.73~99.77%, and 100.81~102.63%, individually. Separate titrations of **CA-AuCu NCs** with Cr(VI) ions and DA in Tap, Lake, Sea, and spiked urine water also experience the fluorescence quenching as displayed in Figs. S26 and S27 (ESM). However, the DA detection in sea water is strongly affected than the others, which is attributed to the salts presented in the medium. The linear regressions of Cr(VI) ions in

Table 1 The recovery values of spiked Cr(VI) ions in real/urine samples and the relative standard deviation (RSD) and ICP-MS values

Sample	Spiked (μM)	Detected [mean ± SD, μM ($n = 3$)]	Recovery (%)	RSD (%)	ICP-MS observed (μM)
Tab water	0.05	0.052 ± 0.006	116.01	1.73	0.0517
	0.50	0.541 ± 0.011	110.42	0.86	0.532
	100	112.21 ± 0.022	112.23	1.41	110.5
Lake water	0.1	0.109 ± 0.007	109.03	1.27	0.11
	0.25	0.267 ± 0.025	116.41	1.05	0.259
	100	114.8 ± 0.011	114.99	2.13	111.3
Sea water	0.05	0.0523 ± 0.008	106.22	2.17	0.053
	0.05	0.537 ± 0.033	114.03	1.64	0.543
	50	56.16 ± 0.018	112.36	0.83	59.2
Urine	0.2	0.232 ± 0.004	118.02	0.97	0.228
	1	1.137 ± 0.026	116.34	2.04	1.152
	25	27.56 ± 0.015	110.29	1.12	26.86

tab/lake/sea/urine samples are found to be 0.3 160, 0.4 160, 0.5 100 and 0.2 120 μM, individually. Likewise, linear regressions of DA in tab/lake/sea/urine samples are established as 1 300, 1 500, 50 600 and 0.4 700 μM, independently. From standard deviation and linear fittings and 3σ [signal to noise, $n = 4$; Figs. S28 and S29 (ESM)], the LODs of Cr(VI) ions and DA in those real samples are estimated. The LODs of Cr(VI) in tap, lake, sea, and urine samples are determined to be 99, 106, 114, and 85 nM, correspondingly. The LODs of DA in tap, lake, sea, and urine samples are calculated as 171 nM, 223 nM, 1.465 μM, and 206 nM, respectively. Table S5 (ESM) summarizes the linear ranges and LODs of Cr(VI) and DA which prove their successful detection in real and urine samples. Photographs of time and concentration dependent fluorescent and visual changes of **CA-AuCu NCs** to Cr(VI) and DA in real/urine samples are displayed in Figs. S30-S37 (ESM).

Cellular imaging of Cr(VI) and DA

Before moving on to cell imaging, the cytotoxicity of **CA-AuCu NCs** is established in Fig. S38a (ESM). In which, **CA-AuCu NCs** demonstrate the viability of 80% even at a concentration of 60 μg/mL, and hence prove low in toxicity [35]. The IC_{50} value of **CA-AuCu NCs** is predicted as 149 μg/mL as displayed in Fig. S38b (ESM). Upon incubation of those low toxic **CA-AuCu NCs** with Raw 264.7 cells, bright blue luminescent cell lines are visualized as shown in Fig. 4. These luminescent cells are then stained with Cr(VI) or DA and incubated for either 30 or 60 min. Once stained and incubated, luminescence in cells begins to quench. Therefore, we conclude that **CA-AuCu NCs**-based Cr(VI) and DA detection can be done in bio-samples. Moreover, in compared to earlier diverse methods, Tables S6 and S7 (ESM) show that Cr(VI) and DA discriminations are equally effective in terms of detection methods, linear ranges, LODs and applicability.

Table 2 The recovery values of spiked DA in real/urine samples and the relative standard deviation (RSD) values

Sample	Spiked (μM)	Detected [mean ± SD, μM ($n = 3$)]	Recovery (%)	RSD (%)
Tab water	100	99 ± 0.93	99.92	2.16
	400	401 ± 0.33	100.33	3.11
	700	698 ± 0.45	99.78	1.67
Lake water	200	202 ± 0.9	101.45	2.08
	500	492 ± 0.27	98.45	1.74
	800	799 ± 0.81	99.98	3.42
Sea water	500	493 ± 0.67	98.73	3.31
	900	897 ± 0.92	99.77	1.02
	1500	1491 ± 0.89	99.45	1.32
Urine	300	302 ± 0.42	100.81	0.63
	600	615 ± 0.76	102.63	1.01
	900	921 ± 0.55	102.39	2.71

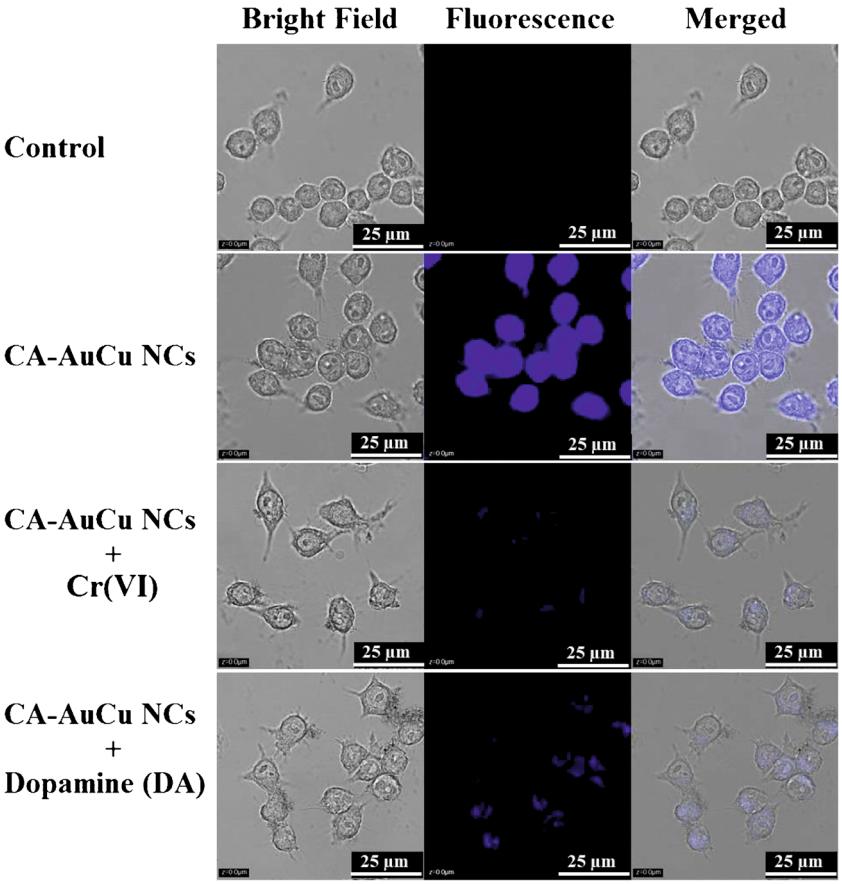

Fig. 4 Cellular imaging of **CA-AuCu NCs** in presence of Cr(VI) ions and dopamine (DA) in Raw 264.7 cell lines (scale: 0–25 µm)

Conclusion

Highly emissive low toxic cysteamine capped gold-copper nanoclusters (**CA-AuCu NCs)** were synthesized via one-pot anti-galvanic reduction approach and employed in the detections of Cr(VI) ions and dopamine (DA) in real/urine samples. Notably, Cr(VI) ions and DA quantifications can be distinguished by their visual and fluorescent responses. However, DA detection is still limited to complex samples consist of higher volume of tyrosine or ascorbic acid as interferences. Demonstrated cellular imaging utilities and diverse aggregation/electron transfer mechanisms on Cr(VI) and DA assays may contribute to design such unique analytical probes.

Acknowledgements The authors are grateful to the Ministry of Science and Technology of Taiwan for financially supporting this research under the contract MOST 107-2811-M-009-015 and MOST 105-2112-M-009-005-MY3.

Compliance with ethical standards

Conflicts of interest Diluted spiked urine samples used in this study are remnants of our earlier reports and not clinical/collected from any volunteer. The cell lines were provided by the Food Industry Research and Development Institute (Taiwan). The author(s) declare that they have no competing interests.

References

1. Zhang H-Y, Wang Y, Xiao S, Wang H, Wang J-H, Feng L (2017) Rapid detection of Cr(VI) ions based on cobalt(II)-doped carbon dots. Biosens Bioelectron 87:46–52
2. Song J, Zhou H, Gao R, Zhang Y, Zhang H, Zhang Y, Wang G, Wong PK, Zhao H (2018) Selective determination of Cr(VI) by Glutaraldehyde cross-linked chitosan polymer Fluorophores. ACS Sens 3:792–798
3. Rasheed PA, Lee J-S (2017) Recent advances in optical detection of dopamine using nanomaterials. Microchim Acta 184:1239–1266
4. Zhang X, Liu W, Li X, Zhang Z, Shan D, Xia H, Zhang S, Lu X (2018) Ultrahigh selective colorimetric quantification of chromium(VI) ions based on gold amalgam catalyst Oxidoreductase-like activity in water. Anal Chem 90:14309–14315
5. Gualandi I, Tonelli D, Mariani F, Scavetta E, Marzocchi M, Fraboni B (2016) Selective detection of dopamine with an all PEDOT:PSS organic electrochemical transistor. Sci Rep 6:35419
6. Patriarchi T, Cho JR, Merten K, Howe MW, Marley A, Xiong W-H, Folk RW, Broussard GJ, Liang R, Jang MJ, Zhong H, Dombeck D, Zastrow MV, Nimmerjahn A, Gradinaru V, Williams JT, Tian L (2018) Ultrafast neuronal imaging of dopamine dynamics with designed genetically encoded sensors. Science 360:eaat4422
7. Gómez V, Callao MP (2006) Chromium determination and speciation since 2000. TrAC Trends Anal Chem 25:1006–1015

8. Unceta N, Séby F, Malherbe J, Donard OFX (2010) Chromium speciation in solid matrices and regulation: a review. Analy Bioana Chem 397:1097–1111
9. Perry M, Li Q, Kennedy RT (2009) Review of recent advances in analytical techniques for the determination of neurotransmitters. Anal Chim Acta 653:1–22
10. van Staden JF, van Staden RIS (2012) Flow-injection analysis systems with different detection devices and other related techniques for the in vitro and in vivo determination of dopamine as neurotransmitter. A review. Talanta 102:34–43
11. Wu D, Sedgwick AC, Gunnlaugsson T, Akkaya EU, Yoon J, James TD (2017) Fluorescent chemosensors: the past, present and future. Chem Soc Rev 46:7105–7123
12. Ma Y, Chen Y, Liu J, Han Y, Ma S, Chen X (2018) Ratiometric fluorescent detection of chromium(VI) in real samples based on dual emissive carbon dots. Talanta 185:249–257
13. Jiang Y, Wang B, Meng F, Cheng Y, Zhu C (2015) Microwave-assisted preparation of N-doped carbon dots as a biosensor for electrochemical dopamine detection. J Colloid Interface Sci 452:199–202
14. Xu W, Yu L, Xu H, Zhang S, Xu W, Lin Y, Zhu X (2019) Water-dispersed silicon quantum dots for on-off-on fluorometric determination of chromium(VI) and ascorbic acid. Microchim Acta 186: 673
15. Liu S, Shi F, Zhao X, Chen L, Su X (2013) 3-Aminophenyl boronic acid-functionalized CuInS2 quantum dots as a near-infrared fluorescence probe for the determination of dopamine. Biosens Bioelectron 47:379–384
16. Zhang JR, Zeng AL, Luo HQ, Li NB (2016) Fluorescent silver nanoclusters for ultrasensitive determination of chromium(VI) in aqueous solution. J Hazard Mater 304:66–72
17. Qu F, Liu Y, Kong R, You J (2017) A versatile DNA detection scheme based on the quenching of fluorescent silver nanoclusters by MoS2 nanosheets: application to aptamer-based determination of hepatitis B virus and of dopamine. Microchim Acta 184:4417–4424
18. Mutuyimana FP, Liu J, Nsanzamahoro S, Na M, Chen H, Chen X (2019) Yellow-emissive carbon dots as a fluorescent probe for chromium(VI). Microchim Acta 186:163
19. Cui M, Wang C, Yang D, Song Q (2017) Fluorescent iridium nanoclusters for selective determination of chromium(VI). Microchim Acta 185:8
20. Liu X, Zhang W, Huang L, Hu N, Liu W, Liu Y, Li S, Yang C, Suo Y, Wang J (2018) Fluorometric determination of dopamine by using molybdenum disulfide quantum dots. Microchim Acta 185:234
21. Shellaiah M, Sun KW (2017) Luminescent metal Nanoclusters for potential Chemosensor applications. Chemosensors 5:36
22. Kang H, Kim B-G, Na HB, Hwang S (2015) Anti-galvanic reduction of silver ion on gold and its role in anisotropic growth of gold Nanomaterials. J Phys Chem C 119:25974–25982
23. Sun J, Wu H, Jin Y (2014) Synthesis of thiolated Ag/au bimetallic nanoclusters exhibiting an anti-galvanic reduction mechanism and composition-dependent fluorescence. Nanoscale 6:5449–5457
24. Bao Z, Zhang K, Jian J, Hu Z, Yuan K, Shao H, Peng K, Jiang Z, Zapien JA, Yan Y, Zhang C, Zhou H (2018) Strongly fluorescent cysteamine-coated copper nanoclusters as a fluorescent probe for determination of picric acid. Microchim Acta 185:507
25. Shellaiah M, Simon T, Venkatesan P, Sun KW, Ko F-H, Wu S-P (2017) Nanodiamonds conjugated to gold nanoparticles for colorimetric detection of clenbuterol and chromium(III) in urine. Microchim Acta 185:74
26. Zhang X, Zhao H, Xue Y, Wu Z, Zhang Y, He Y, Li X, Yuan Z (2012) Colorimetric sensing of clenbuterol using gold nanoparticles in the presence of melamine. Biosens Bioelectron 34:112–117
27. Pakiari AH, Jamshidi Z (2010) Nature and strength of M−S bonds (M = au, Ag, and cu) in binary alloy gold clusters. J Phys Chem A 114:9212–9221
28. Wilcoxon JP, Abrams BL (2006) Synthesis, structure and properties of metal nanoclusters. Chem Soc Rev 35:1162–1194
29. Liu M, Zhou W, Wang T, Wang D, Liu L, Ye J (2016) High performance au–cu alloy for enhanced visible-light water splitting driven by coinage metals. Chem Commun 52:4694–4697
30. Yang X, Feng Y, Zhu S, Luo Y, Zhuo Y, Dou Y (2014) One-step synthesis and applications of fluorescent cu nanoclusters stabilized by l-cysteine in aqueous solution. Anal Chim Acta 847:49–54
31. Goswami N, Giri A, Bootharaju MS, Xavier PL, Pradeep T, Pal SK (2011) Copper quantum clusters in protein matrix: potential sensor of Pb2+ ion. Anal Chem 83:9676–9680
32. Das NK, Ghosh S, Priya A, Datta S, Mukherjee S (2015) Luminescent copper Nanoclusters as a specific cell-imaging probe and a selective metal ion sensor. J Phys Chem C 119:24657–24664
33. Noh M, Kim T, Lee H, Kim C-K, Joo S-W, Lee K (2010) Fluorescence quenching caused by aggregation of water-soluble CdSe quantum dots. Colloids Surf A Physicochem Eng Asp 359: 39–44
34. Govindaraju S, Ankireddy SR, Viswanath B, Kim J, Yun K (2017) Fluorescent gold Nanoclusters for selective detection of dopamine in cerebrospinal fluid. Sci Rep 7:40298
35. Song X-R, Goswami N, Yang H-H, Xie J (2016) Functionalization of metal nanoclusters for biomedical applications. Analyst 141: 3126–3140

Publisher's note Springer Nature remains neutral with regard to jurisdictional claims in published maps and institutional affiliations.